Distinguishability of Battery Equivalent-Circuit Models Containing CPEs: Updating the Work of Berthier, Diard, & Michel

Eden Poihipi[a], Jonathan Scott[a] and Christopher Dunn[a]

[a]University of Waikato, Private Bag 3105, Hamilton 3240, New Zealand

ARTICLE INFO

Keywords:
Constant Phase Elements
Equivalent Circuit Model
Battery Model
Frequency Response
EIS

ABSTRACT

This manuscript revisits the assertion of Berthier et al. that competing fractional-element equivalent-circuit models of battery cells are indistinguishable in the presence of noise. Starting with Westerhoff's general equivalent-circuit model (ECM) of 2016 and an idealized impedance spectrum of a lithium battery, a contemporary set of possible ECMs are chosen. Their distinguishability is investigated. Using the extended frequency range recommended by Mauracher & Karden in 1997 or Hasan & Scott in 2019, an approach is presented that permits selection of the appropriate model, even in the presence of noise. For the given frequency range, models with up to five elements or eight real parameters are studied. Fitting to measured data with straightforward numerical methods and choosing the most primitive appropriate sub-circuit is shown to reproduce the data. Typically a three-element, five-parameter ECM is shown to model real, measured data with precision comparable to individual sample error.

1. Introduction

Electrochemists seek the equivalent-circuit model (ECM) of a battery to characterize its internal processes, while electrical engineers seek the same model in order to predict state-of-charge (SoC) and state-of-health (SoH). There is today a vast amount of literature in which models are presented and applied.

Berthier et al. [1] presented a paper in 2001 that set out to determine from an electrochemical perspective whether ECMs containing constant phase elements (CPEs) were numerically distinguishable from one another. These authors used CPEs in models based on electrochemical impedance spectroscopy (EIS) data, and explored their hypothesis by numerically fitting four arbitrary ECMs to synthesized EIS data using the optimization method of Fletcher et al. [2]. They concluded that the ECMs are distinguishable provided that the synthesized EIS data are noise-free. Each circuit was further optimized against noisy synthesized EIS data using 0%, 1%, 2.5% and 5% noise. The authors concluded that circuits became indistinguishable from one another once the noise level exceeded 1%.

Berthier's group used angular frequencies from 100 radians/s (16 Hz) to 1 Mrad/s (160 kHz), and displayed results in the form of Argand diagrams (sometimes called Nyquist plots). These frequency bounds and mode of presentation impose significant limitations. Moreover, optimization was applied without delving into details of the process, and equally for each ECM irrespective of its complexity.

Batteries in appliances such as cellphones, computers, and vehicles are commonly cycled as infrequently as once a week or longer, and certainly no more often than every few minutes. These periods equate roughly to frequencies ranging from 1 µHz to 1 mHz, or equivalently C-rates from 0.006 to 4. In the case of rechargeable batteries, this implies the need to measure at extra low frequencies (ELFs) to encompass typical usage patterns [3, 4, 5].

This manuscript aims to update the work of Berthier and colleagues, with use of an expanded frequency range and presentation of data in Bode plot form. This offers advantages where frequency information is important [6]. In addition, a guided fitting process will be used, and a progressive set of ECMs will be drawn from recent literature [7, 8].

2. Battery Equivalent-Circuit Models

Westerhoff and colleagues [7] suggested that there are three ways to characterize a battery, referred to as 'black,' 'gray' and 'white' box models. White box is a theoretical modelling method which returns to fundamental physics and a detailed understanding of the physical chemistry to determine behavior potentially leading to an ECM [9]. For example, [10] starts with white-box methods, than transitions to grey-box models through the fitting of an ECM. Black box modelling, on the other hand, employs a blind empirical modelling method using sets of measured data to extract a battery model [11]. This method works best for linear relationships and is not often used on its own [9] since model extraction requires large, accurate, data sets and computationally intensive software [11]. Gray box modelling is the combination of the White and Black methods, using both theoretical understanding of the system and measured data for a more reliable model [10, 11].

Westerhoff and colleagues [7] described 'gray' box modeling, in which quantitative ECMs were generated on the basis of experimental data. Westerhoff et al. presented a general battery model (Figure 1). Like Berthier 15 years before him, Westerhoff includes CPEs, sometimes identified as "fractional capacitors", in his model. Since Randles in 1947 [12], electrochemists have acknowledged the presence of these fractional-derivative functions in their models. Conversely, the engineering literature contains many ECM models that

ORCID(s):

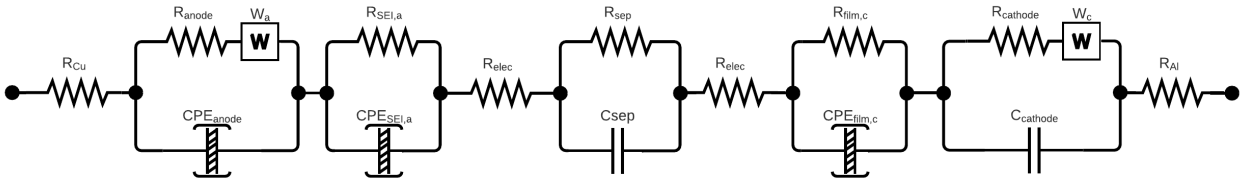

Figure 1: Potential complete equivalent circuit of a battery according to Westerhoff [7]. Constant phase elements (CPEs) are used to characterize electrochemical behavior at the anode, solid electrolyte interface (SEI), separator (sep), and cathodic thin film (film,c). Note also resistances (R) associated with the copper and aluminium foils (Cu and Al), anode, SEI, electrolyte (elec), separator, thin film and cathode, and capacitances (C) at the separator and cathode. Warburg elements are denoted by W_a and W_c at the anode and cathode, respectively.

are based at best on second-(integral)-order models [13], despite it having been shown that they are not appropriate[14]. The separate electrical and electrochemical components in a battery are represented by individual circuits, each connected in series with the others. The manuscript suggested that this general model can be simplified leaving fewer sub-circuits while continuing to represent the characteristics of a battery, depending upon the significance of each component to the whole impedance. The authors then compared the output impedance spectra of these sub-circuits to data obtained experimentally. They concluded that the chief determinant of the number of components required for each sub-circuit was the accuracy required for the application in question. Hence, it is possible to reduce the number of components in Figure 1 without losing the ability to represent the impedance output of a rechargeable battery accurately.

In this manuscript six ECMs will be considered. They will be used in a progressive model fitting approach. The distinguishability and performance of each of the ECM sub-circuits is explored by numerically fitting each one to simulated battery data. The six ECMs appear in Figure 2.

The first ECM reduces the Westerhoff circuit to its simplest form. This ECM contains two elements: a single CPE and a series resistor. (Figure 2, upper left circuit.) The impedance of an ideally polarizable liquid electrode (e.g. mercury, amalgam, or indium-gallium) can be modeled by an R-C circuit, but the double-layer capacitance of a solid electrode is not purely capacitative, displays frequency dispersion, and cannot be modeled adequately by an ECM based on capacitors [15]. Instead, CPEs are used to emulate this non-ideally polarizable behavior. The equation for the impedance of a CPE is

$$Z_{CPE} = \frac{1}{C_F s^{\alpha}} \tag{1}$$

where C_F is the CPE value (its pseudo- or fractional capacitance, a constant with the dimensions $Fs^{\alpha-1}$), α is the CPE fractional order exponent, $s = j2\pi f$ (where $2\pi f = \omega$, the angular frequency), and f is the frequency in hertz [16]. The total impedance of the R-CPE model can therefore be found by

$$\begin{aligned} Z_{R-CPE} &= R_s + Z_{CPE} \\ &= R_s + \frac{1}{C_F s^{\alpha}} \end{aligned} \tag{2}$$

where R_s is the series resistance and Z_{CPE} is the impedance of the CPE (Equation 1) in ohms.

It is worth mentioning at this point how the particular six sub-circuits have been selected. Why these six, given the large choice afforded by starting with the circuit of Figure 1?

The choice is guided by measured impedance data. Figure 3 shows the magnitude and phase of impedance measured on a small selection of batteries covering different chemistries and capacities. The traces all share a basic shape associated with the base R-CPE circuit. As will become clear below, the other circuits that we have chosen to use in this study correspond to characteristics observed in at least a few measured examples.

The R-CPE model can be extended by the addition of a Warburg element (W) to become the second ECM, R-CPE-W. (Figure 2, upper right circuit.) Warburg elements are CPEs with an alpha bound to a value of one-half. They famously appeared in the electrode reaction experiments of Randles reported in 1947 [12], and describe Faradaic impedance in the presence of redox processes in semi-infinite linear diffusion systems [6]. Their generalization to arbitrary fractional order yields the CPE described above [17]. The impedance of a Warburg element is given by

$$Z_{\text{Warburg}} = \frac{1}{C_W s^{\frac{1}{2}}} \tag{3}$$

and so the impedance of the R-CPE-W model is given by

$$\begin{aligned} Z_{\text{R-CPE-W}} &= R_s + Z_{CPE} + Z_{\text{Warburg}} \\ &= R_s + \frac{1}{C_F s^{\alpha}} + \frac{1}{C_W s^{\frac{1}{2}}} \end{aligned} \tag{4}$$

where R_s is the series resistance, Z_{CPE} is the impedance of the CPE (Equation 1) and Z_{Warburg} is the impedance of the Warburg element (Equation 3).

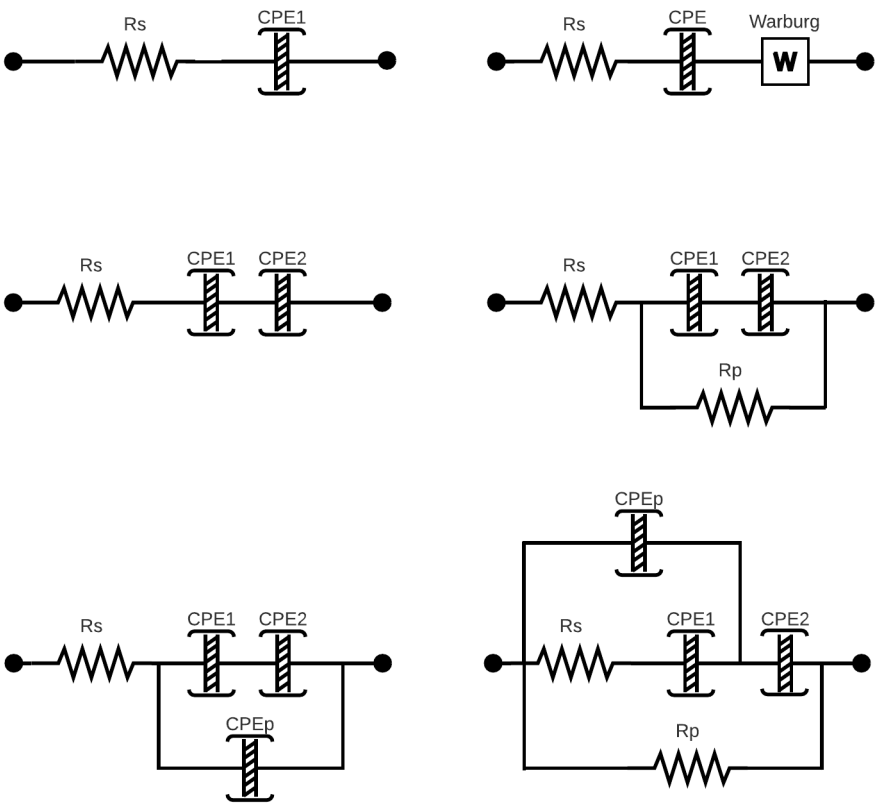

Figure 2: The equivalent-circuit models (ECMs) considered in this manuscript. For ease of communication we identify them by the sequence of elements. The top left circuit can be identified as "R-CPE", the top right as "R-CPE-W", the middle left as "R-CPE-CPE", middle right as "R-CPE-CPE-Rp", then "R-CPE-CPE-CPEp" and finally "R-CPE-CPE-Rp-CPEp".

In practice, assumptions made in the theory that anticipates a Warburg element are often not completely met. The Warburg can be replaced by a CPE to give an extra degree of freedom. (Figure 2, middle left circuit, and so forth.) The total impedance of this model is given by

$$\begin{aligned} Z_{\text{R-CPE-CPE}} &= R_s + Z_{\text{CPE1}} + Z_{\text{CPE2}} \\ &= R_s + \frac{1}{C_F s^{\alpha}} + \frac{1}{C_W s^{\alpha_2}} \end{aligned} \tag{5}$$

where R_s is the series resistance, and Z_{CPE1} and Z_{CPE2} are the impedances of the two CPEs, and we keep the W subscript to show the origin of the element.

Readers familiar with circuit theory will appreciate that small phase deviations at high and low frequency extents suggest a parallel element in the mix. Additional components can be added in parallel with other elements in an ECM to accommodate deviations in battery phase response. The R-CPE-CPE-Rp subcircuit will have impedance

$$Z_{\text{R-CPE-CPE-Rp}} = R_s + \left[Z_{\text{CPE1}} + Z_{\text{CPE2}}\right] \parallel R_p \tag{6}$$

where R_p is the parallel resistance. This equation can be expanded by noting that the impedance of parallel elements can be written

$$X \parallel Y = \frac{1}{\frac{1}{X} + \frac{1}{Y}} = \frac{XY}{X+Y} \tag{7}$$

leading to

$$Z_{\text{R-CPE-CPE-Rp}} = \frac{\left[R_s + Z_{\text{CPE1}} + Z_{\text{CPE2}}\right] R_p}{R_s + Z_{\text{CPE1}} + Z_{\text{CPE2}} + R_p} \tag{8}$$

and then

$$Z_{\text{R-CPE-CPE-Rp}} = \frac{\left[R_s + \frac{1}{C_F s^{\alpha}} + \frac{1}{C_W s^{\alpha_2}}\right] R_p}{R_s + \frac{1}{C_F s^{\alpha}} + \frac{1}{C_W s^{\alpha_2} + R_p}}. \tag{9}$$

The form of (6) is usually preferred by engineers over (9) because it is more intuitive and easier to assimilate. As the expansions rapidly become more onerous we will restrict ourselves to the parallel notation from here onwards.

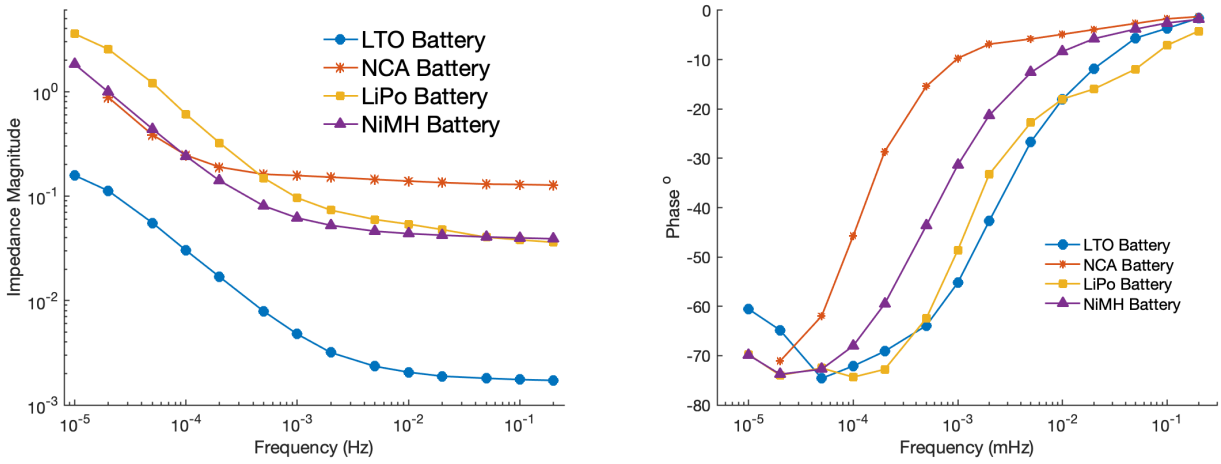

Figure 3: Impedance magnitude of a selection of rechargeable batteries. LTO is a lithium titanate cell of 40 Ah capacity, NCA is a 4.8 Ah lithium nickel cobalt aluminium cell, LiPo is a 250 mAh lithium polymer cell, and NiMH is a 2.5 Ah nickel-metal hydride cell.

The final two ECMs to be investigated have impedances Z_5 and Z_6

$$\begin{aligned} Z_5 &= Z_{\text{R-CPE-CPE-CPEp}} \\ &= R_s + \left[Z_{\text{CPE1}} + Z_{\text{CPE2}}\right] \parallel Z_{\text{CPEp}} \\ &= R_s + \left[\frac{1}{C_F s^{\alpha}} + \frac{1}{C_W s^{\alpha_2}}\right] \parallel \frac{1}{C_P s^{\alpha_p}} \end{aligned} \tag{10}$$

where the $\parallel$ operator is taken to have precedence over addition, α_p is the order of the parallel CPE, and C_P the proportionality constant of the parallel CPE; and

$$\begin{aligned} Z_6 &= Z_{\text{R-CPE-CPE-Rp-CPEp}} \\ &= \left[\left[R_s + Z_{\text{CPE1}}\right] \parallel Z_{\text{CPEp}} + Z_{\text{CPE2}}\right] \parallel R_p \\ &= \left[\left[R_s + \frac{1}{C_F s^{\alpha}}\right] \parallel \frac{1}{C_P s^{\alpha_p}} + \frac{1}{C_W s^{\alpha_2}}\right] \parallel R_p \end{aligned} \tag{11}$$

3. Fitting Algorithm

Following the lead of Berthier and colleagues [1], data will be generated from one of the ECMs with varying amounts of numerical noise, and each model will be fitted to that data.

3.1. Numerical Optimization Method

The numerical optimizer was created in Matlab, using both the inbuilt toolboxes and previously published examples of real-parameter black box optimization algorithms [18, 19, 20]. The optimization method utilizes the downhill simplex algorithm of Nelder & Mead [21, 22], a direct-search method which aims to minimize non-linear, multidimensional functions. For a function with n dimensions, the optimizer takes a set of $n + 1$ vertices to create a simplex. The vertices then move iteratively in order to reduce the size of the simplex until a termination value is reached. The main limitation of the Nelder-Mead approximation is potential for convergence of the simplex to local minimum, called a 'saddle', rather than the global minimum.

The method is analogous to multiple skiers on a mountain. As the $n+1$ skiers traverse downward on various paths, they all end up at the lowest point in their environment. However, each skier may end up at different locations and elevations when they reach the 'bottom'. One way to address this problem is to have multiple random starting points and then evaluate which starting point minimized the function the furthest. In some cases we applied this approach using a second program written in C. The C program could apply thousands of random multiple starts with variable range of starting points in a period of about a minute.

The root-mean-square error (RMSE) used as the optimization goal is calculated from the impedances defined in equations (2–11) above. Impedance values are complex, and the RMSE is defined as the square root of the average of the squared distance in the complex impedance (Argand) plane. Various alternatives, weighting magnitude and phase differently, etc., were tried, but proved to offer no advantages.

3.2. Fitting Sequence

Choosing the appropriate model to fit given data commences with the simplest ECM, the R-CPE model. The model has only three parameters, converges quickly, and generally finds the global minimum without restarts. The final root-mean-square error (RMSE) reflects how well the model fits the data. If the model perfectly fits ideal data, the RMSE will approach zero. If the model perfectly fits data with a certain amount of random white noise, the RMSE will settle at a value close to that noise level, so that 1% added noise will result in a final RMSE of about 0.01. If the model does not fit the data, the extent of the mismatch also appears in the RMSE.

The second step of the model selection process moves to the next-simplest model, in this case the R-CPE-W model, with four parameters. The fit starts at the model parameter

Table 1
Synthetic Model Parameter Values

Parameter	R_s	α	C_F	C_W	$\alpha 2$
Value	0.05	0.75	10,000	500	0.40
Parameter	R_p	α_p	C_p		
Value	500	0.15	0.8		

values returned in the R-CPE case. If the previous fit has settled at a point where the RMSE was largely defined by noise in the data, then this attempt will not improve upon the fit, and it may be concluded that the quality of the data does not justify this more complicated model, even if that model might be more correct. However, if the added element results in a lower RMSE, it must be concluded that the extended model does represent the data better.

This process is repeated for the ECMs with increasing degrees of freedom, the R-CPE-CPE model, with five parameters, in the third step, and so on. During the progressive fitting, it is possible for parameter values to be returned that are impossible. For example, α cannot exceed 1.0, and C_p cannot be negative. Such an event signals that the model and fit cannot be appropriate for the data.

4. Simulated Data

A set of model parameter values were chosen for the ECM with eight degrees of freedom, the R-CPE-CPE-Rp-CPEp model. Values appear in Table 1. The magnitude and phase computed using Equation 11 are plotted in Figure 4. Also plotted in the figure are the asymptotes corresponding to each of the five elements. This permits the reader to associate regions in the plot with different elements; for example, the horizontal section of the magnitude plot between 1 mHz and 1 Hz is dominated by the series resistance, R_s, and the straight-line region between 1 µHz and 20 µHz is dominated by the first CPE. A practised eye can pick up other hints about what ECM might be appropriate. For example, the curling up of the phase below 1 µHz hints at a parallel element, and the rounded, gradual nature of the corner at 500 µHz hints at a second fractional series element.

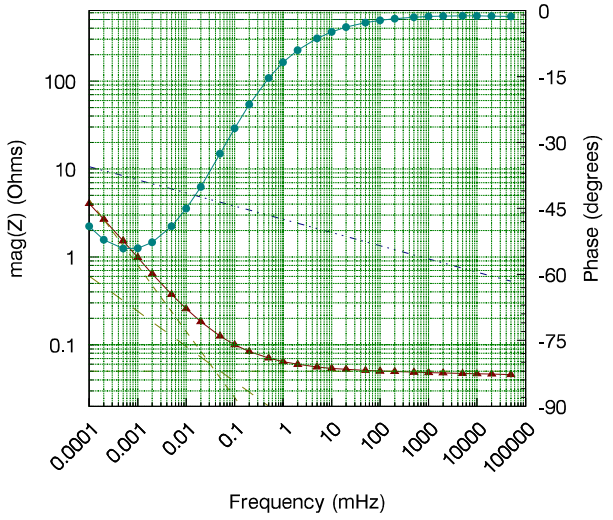

Figure 4: Plot of magnitude (red triangles) and phase (cyan dots) generated from the eight-parameter model. The additional straight lines represent the impedance of the five elements of the model, three CPEs plus series and parallel pure resistance.

5. Model Discrimination & Selection

Figure 5 depicts the RMSE obtained fitting each of the ECMs to ideal noiseless data computed according to Section 4. The result is not surprising; only the correct model yields the expected RMSE of zero. Nevertheless, it is also possible to say that the parallel elements are having much less impact on the fit than the three series elements. Also note that the extra degree of freedom acquired when the Warburg is allowed to become a CPE significantly improves the fit, something that might not be expected from the position of its asymptote in Figure 4.

Adding noise at 1% and 3% leads to the results in Figure 6. This plot contain a great deal of information. The noiseless data from Figure 5 is reproduced adjacent to the noisy results for comparison. As expected, adding noise increases the RMSE in all cases. Error bars have been added to the noisy RMSE results. In each case 30 simulations were run with different added noise, and the mean and standard deviation (SD) of the RMSE calculated across these runs. The error bars show the ±1.0 SD extents.

Observe that the RMSE results do vary somewhat for given noise contribution, but not greatly. Where different models return RMSE values that lie within the error margins, the conclusion must be that the models are indistinguishable. One way of interpreting this is to say that the quality of the data does not justify the added complexity of the model with a higher number of degrees of freedom. In the example, the R-CPE-CPE-Rp model has six degrees of freedom, the R-CPE-CPE-CPEp model seven, and the R-CPE-CEP-Rp-CPEp model eight. It is clear that the first three models (with three, four, and five degrees of freedom) all fall short of the final three. Amongst the final three, the R-CPE-CPE-Rp model, as the most constrained, is to be preferred. This conclusion is reached both in the case of 1% noise, and 3% added noise. In other words, once noise reaches as little as 1% it becomes impossible to distinguish between the final three models. Given the RMSE with incorrect models but operating with noise-free data, it can be anticipated that the last three models will become indistinct when noise reaches about half a percentage point.

6. Measured Data

The modelling process described above was applied to impedance magnitude and phase data measured on real batteries. Measured data were obtained for a near-new lithium nickel cobalt aluminium oxide (referred to variously as NCA or NCR) 21700 cell and a used but healthy lithium nickel

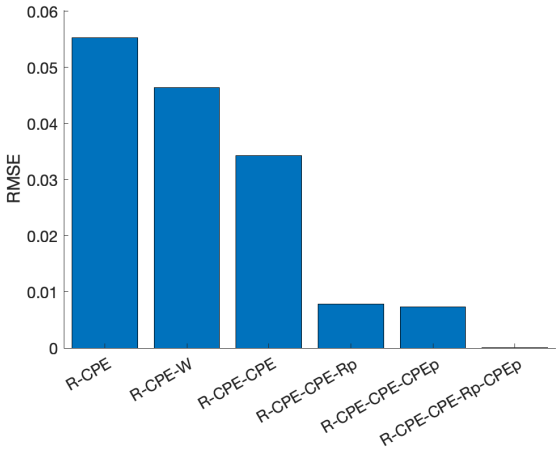

Figure 5: RMS error obtained fitting the various equivalent-circuit models to ideal (noiseless) synthesized data.

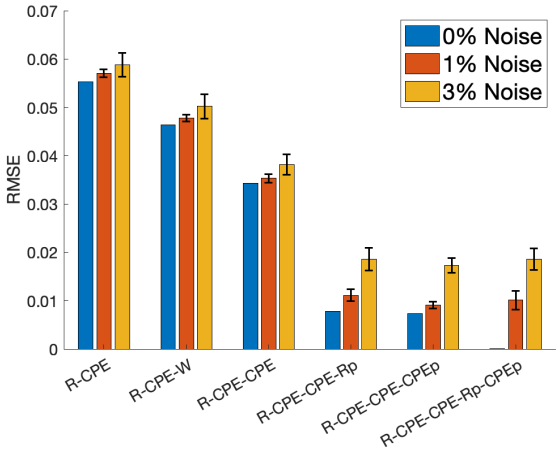

Figure 6: RMS error obtained fitting the various equivalent-circuit models to ideal (noiseless), 1 percent noise, and 3 percent noise synthesized data. Error bars show 1 standard deviation in expected RMS error.

manganese cobalt oxide (referred to variously as NMC or INR) 18650 cell. Measurements are made with a developed form of the method initially described by Scott and Hasan [4]. For the present experiment, a multiple-sinewave current consisting of multiple frequencies ranging between 0.5 µHz and 2 Hz was delivered using a two-quadrant power supply (model 66332A dynamic measurement source) controlled by software developed in-house, written in C, and running on a Raspberry Pi 4 connected via a Prologix-compatible open-source GPIB interface. The 66332A delivers up to 5 A of current, and has voltage and current resolutions of 5 mV and 1.32 mA, respectively. The software can be configured to distribute either current or charge displacement across all frequencies in various fashions.

Impedance, Z, of an electrochemical system around some steady or quasi-steady state can be determined by:

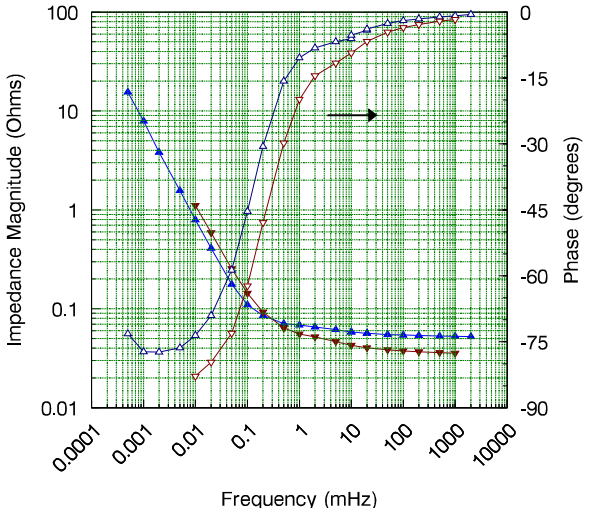

Figure 7: Plot of measured impedance magnitude (solid blue up triangles) and phase (open blue up triangles) of a lithium nickel cobalt aluminium oxide (NCR/NCA) 2170 cell and magnitude (solid red down triangles) and phase (open red down triangles) measured on a lithium nickel manganese cobalt oxide (INR/NMC) 18650 cell.

1. applying a small-signal multitonal sinusoidal current, where $I(t) = |I|e^{j(\omega t+\phi_I)}$;
2. measuring the voltage response $V(t) = |V|e^{j(\omega t+\phi_V)}$;
3. calculating $Z(\omega) = \frac{|V|}{|I|}e^{j(\phi_V-\phi_I)}$) [23].

$Z(\omega)$ is made up of real and imaginary parts:

$$Z(\omega) = Z_0\cos(\phi) + jZ_0\sin(\phi)$$

where $Z'_{real} = Z_0\cos(\phi)$, the resistance of the system, and $Z''_{imag} = Z_0\sin(\phi)$, capacitance and/or inductance, representing energy storage [8]. In this manuscript, we display Bode plots which present magnitude $|Z(\omega)| = |V|/|I|$ and phase $\arg(Z(\omega)) = \phi_V - \phi_I$.

Current and voltage were logged by the 66332A approximately every 0.1 s. Magnitudes and phases of both parameters at the frequencies of interest, required to permit the above calculations, were determined using a discrete Fourier transform (DFT) after the method first described by Scott and Parker [24]. The resulting magnitude and phase plots for the batteries used here are shown in Figure 7.

The results of attempting to fit the various ECMs to these batteries appear in Figure 8. The associated model parameters appear in Tables 2 and 3.

Observing the RMSE for the various models in Figure 8, it is clear for the NMC cell, for which less data is available, that the R-CPE-CPE model is the appropriate choice. More than five degrees of freedom cannot be justified, and the error in the data is relatively small in measurement terms. In the case of the NCA cell, the noise is much larger, but the data span a greater frequency range. The RMSE settles to a value almost triple that of the other cell. Nevertheless, the data clearly justify a six-parameter model, whose parameters appear in Table 3. The more complex models have very

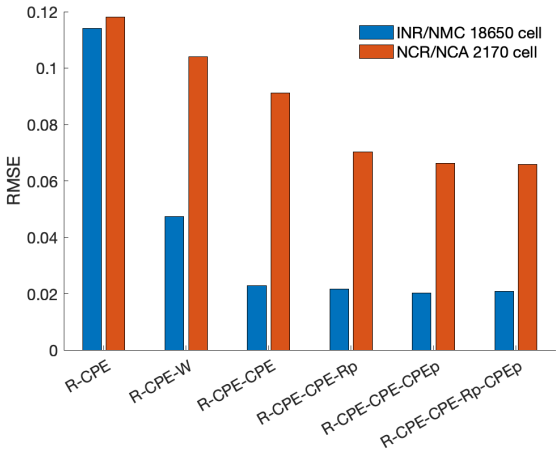

Figure 8: RMS error obtained fitting each ECM to the two data sets presented in Figure 7. The left-hand blue bars correspond to the NMC cell.

Table 2
ECM Parameters for NMC 18650 cell

Parameter	R_s	α	C_F	C_W	$\alpha 2$
Value	0.0330	0.99	14,180	187	0.27

Table 3
ECM Parameters for NCA 2170 cell

Parameter	R_s	α	C_F	C_W	$\alpha 2$	R_p
Value	0.0503	0.99	22,230	230	0.272	44

slightly less RMSE, but not by a margin that we consider to warrant the complexity.

7. Conclusion

We have revisited the work of Berthier, employing fractional equivalent-circuit models inspired by recent, extra-low frequency EIS measurements. Our conclusion is that it *is* possible to distinguish between a selection of ECMs. With real, noisy data there will be models between which it will not be possible to make a reliable selection. We say of these that their extra degrees of freedom are not justified in the face of the quantity and quality of data available. In other words, adding degrees of freedom is not justified if the RMSE does not decrease by an extent greater than the expected uncertainty. Up to that point, the model with more degrees of freedom and lower RMSE is preferred.

The rich literature on gray-box, equivalent-circuit models exposes a disconnect between the work of electrochemists and electrical engineers, the former have great insight into the circuit elements, and the latter the tools to fit and employ them.

It has become clear that a guided fitting approach and multiple restarts in the optimization can help in finding a global minimum, especially in the case of models with more than a few degrees of freedom. When selecting between several ECMs, the most simple is fitted first, and the results of the first fit used as the starting point for fitting the next-most complicated model. Multiple restarts improve the likelihood that the optimization will not be caught in a saddle.

A wide range of frequencies improves the sensitivity of the RMSE to parameters in a given ECM. The frequency range should be chosen appropriately in view of the intended application of the model.

The ability to obtain values for parameters of elements in the ECM of a battery should allow electrochemists to associate internal components of a battery with branches in the ECM. The same ability should allow electrical engineers to observe degradation & ageing in a battery and predict failure well ahead of the event.

References

[1] F. Berthier, J.-P. Diard, R. Michel, Distinguishability of equivalent circuits containing CPEs: Part I. Theoretical part, J. Electroanal. Chem. 510 (1) (2001) 1–11. doi:10.1016/S0022-0728(01)00554-X.

[2] R. Fletcher, C. Xu, Hybrid Methods for Nonlinear Least Squares, IMA J. Numer. Anal. 7 (3) (1987) 371–389. doi:10.1093/imanum/7.3.371. URL https://academic.oup.com/imajna/article-lookup/doi/10.1093/imanum/7.3.371

[3] P. Mauracher, E. Karden, Dynamic modelling of lead/acid batteries using impedance spectroscopy for parameter identification, J. Power Sources 67 (1-2) (1997) 69–84. doi:10.1016/S0378-7753(97)02498-1.

[4] J. Scott, R. Hasan, New Results for Battery Impedance at Very Low Frequencies, IEEE Access 7 (2019) 106925–106930. doi:10.1109/ACCESS.2019.2932094.

[5] R. Hasan, J. Scott, Extending Randles's Battery Model to Predict Impedance, Charge–Voltage, and Runtime Characteristics, IEEE Access 8 (2020) 85321–85328. doi:10.1109/ACCESS.2020.2992771.

[6] A. Lasia, Impedance of the Faradaic Reactions in the Presence of Mass Transfer, in: Electrochemical Impedance Spectroscopy and its Applications, Springer New York, New York, NY, 2014, pp. 85–125. doi:10.1007/978-1-4614-8933-7_4.

[7] U. Westerhoff, K. Kurbach, F. Lienesch, M. Kurrat, Analysis of Lithium-Ion Battery Models Based on Electrochemical Impedance Spectroscopy, Energy Technol. 4 (12) (2016) 1620–1630. doi:10.1002/ente.201600154.

[8] W. Choi, H.-C. Shin, J. M. Kim, J.-Y. Choi, W.-S. Yoon, Modeling and Applications of Electrochemical Impedance Spectroscopy (EIS) for Lithium-ion Batteries, J. Electrochem. Sci. Technol 11 (1) (2020) 1–13. doi:10.33961/jecst.2019.00528.

[9] B. Sohlberg, E. W. Jacobsen, Grey box modelling – branches and experiences, IFAC Proceedings Volumes 41 (2) (2008) 11415–11420.

[10] L. Nugroho, R. Akmeliawati, Comparison of black-grey-white box approach in system identification of a flight vehicle, Journal of Physics Conference Series, IOP Science 1130 (1).

[11] J. Brucker, W. G. Bessler, R. Gasper, Grey-box modelling of lithium-ion batteries using neural ordinary differential equations, Energy Informatics 4 (15).

[12] J. E. B. Randles, Kinetics of rapid electrode reactions, Discuss. Faraday Soc. 1 (1947) 11. doi:10.1039/df9470100011.

[13] W. Cao, S.-L. Wang, C. Fernandez, C.-Y. Zou, C.-M. Yu, X.-X. Li, A novel adaptive state of charge estimation method of full life cycling lithium-ion batteries based on the multiple parameter optimization, Energy Science and Engineering 7 (5) (2019) 1544–1556.

[14] R. Hasan, J. Scott, Application of Swingler's method for analysis of multicomponent exponentials with special attention to non-equispaced data, in: 2016 IEEE 12th International Colloquium on Signal Processing & Its Applications (CSPA), IEEE, Melaka, Malaysia, 2016, pp. 12–15. doi:10.1109/CSPA.2016.7515794. URL http://ieeexplore.ieee.org/document/7515794/

[15] A. Lasia, Dispersion of Impedances at Solid Electrodes, in: Electrochemical Impedance Spectroscopy and its Applications, Springer New York, New York, NY, 2014, pp. 177–201. doi:10.1007/978-1-4614-8933-7_8.

[16] S. Westerlund, L. Ekstam, Capacitor theory, IEEE Trans. Dielect. Electr. Insul. 1 (5) (1994) 826–839. doi:10.1109/94.326654.

[17] T. T. Hartley, J.-C. Trigeassou, C. F. Lorenzo, N. Maamri, Energy Storage and Loss in Fractional-Order Systems, J. Comput. Nonlinear Dyn. 10 (6) (2015) 061006. doi:10.1115/1.4029511.

[18] N. Hansen, Benchmarking the Nelder-Mead downhill simplex algorithm with many local restarts, in: Proceedings of the 11th Annual Conference Companion on Genetic and Evolutionary Computation Conference: Late Breaking Papers, Association for Computing Machinery, Montreal, Québec, Canada, 2009, pp. 2403–2408. URL https://doi.org/10.1145/1570256.1570335

[19] U. M. Sundar, Numerical Optimization Using MATLAB (2015). URL https://www.mathworks.com/content/dam/mathworks/mathworks-dot-com/solutions/automotive/files/in-expo-2015/numerical-optimization-using-matlab.pdf

[20] A. Parkhomenko, Numerical Optimization in MATLAB (2017). URL https://www.andrii-parkhomenko.net/files/Numerical%20optimization%20in%20Matlab.pdf

[21] J. A. Nelder, R. Mead, A Simplex Method for Function Minimization, Comput. J. 7 (4) (1965) 308–313. doi:10.1093/comjnl/7.4.308.

[22] W. H. Press, Numerical recipes in C : the art of scientific computing, 2nd Edition, Cambridge University Press, Cambridge [England] ;, 1992.

[23] C. Zou, L. Zhang, X. Hu, Z. Wang, T. Wik, M. Pecht, A review of fractional-order techniques applied to lithium-ion batteries, lead-acid batteries, and supercapacitors, J. Power Sources 390 (2018) 286–296. doi:10.1016/j.jpowsour.2018.04.033.

[24] J. Scott, A. Parker, Distortion analysis using SPICE, J. Audio Eng. Soc. 43 (12) (1995) 1029–1040.